CALPHAD: Computer Coupling of Phase Diagrams and Thermochemistry 54 (2016) 54–66

Contents lists available at ScienceDirect

CALPHAD: Computer Coupling of Phase Diagrams and Thermochemistry

journal homepage: www.elsevier.com/locate/calphad

# Thermodynamic analysis of dehydrogenation path of Mg–Al–Li–Na alloys

S. Abdessameud [a], M. Medraj [a,b,*]

[a] Department of Mechanical Engineering, Concordia University, 1455 de Maisonneuve Blvd West, Montreal, Quebec, Canada H3G 1M8
[b] Department of Mechanical and Materials Engineering, Masdar Institute of Science and Technology, Masdar City, Abu Dhabi, United Arab Emirates

ARTICLE INFO

*Article history:*
Received 22 March 2016
Received in revised form
3 June 2016
Accepted 3 June 2016

*Keywords:*
Hydrogen storage
Magnesium hydrides
Lithium alanates
Thermodynamic modeling

ABSTRACT

A thermodynamic study on the Mg–Al–Li–Na–H system is conducted in this work in order to investigate its hydrogen storage properties. For that purpose, a thermodynamic database is constructed using the CALPHAD technique. In this work, Li is added to the previously studied Mg–Al–Na–H system and the related binaries (Li–Mg, Li–Na) and ternaries (Al–Li–Mg, Al–Li–H, Li–Mg–H) are reassessed using the Compound Energy Formalism (CEF) for the terminal solid solutions and the Modified Quasichemical Model (MQM) for the liquid phase. The quaternary hydride $Na_2LiAlH_6$ is assessed for the first time. The constructed database is used to calculate de/re-hydrogenation reaction pathways of $MgH_2$–$LiAlH_4$/$Li_3AlH_6$ composites in a wide temperature and pressure ranges. The results are analyzed and compared with the experimental data to better understand and predict the reaction mechanisms. It is shown that Al resulted from the decomposition of $LiAlH_4$/$Li_3AlH_6$ hydrides destabilizes $MgH_2$ by the formation of Mg–Al phases: β and γ, and that LiH does not contribute to these reactions. Only negligible amounts of hydrogen are released from LiH because of the limited solubility of Li (from LiH) in Mg at high temperatures. It is concluded that $MgH_2$–$Li_3AlH_6$ system has better reversibility than $MgH_2$–$LiAlH_4$ system and promising compositions (e.g. 37.09 mol% and 53.65 mol% $MgH_2$ contents) are predicted. Also, a new destabilization reaction is predicted in the system. The $MgH_2$ and $Na_2LiAlH_6$ hydrides destabilize mutually at 308.4 K (35.25 °C) and 1 bar because of the formation of $MgNaH_3$. However, the hydrogen capacity is reduced. It is concluded that Na considerably reduces the hydrogen storage potential of the system.



## 1. Introduction

The present work is a contribution to the search and development of new materials suitable for hydrogen storage applications. In fact, the storage of hydrogen is the most critical issue for the development of hydrogen energy, especially for mobile applications [1]. Significant attention has been devoted to magnesium and its alloys as potential materials for hydrogen storage because of their high hydrogen capacity [2]. Magnesium hydride, $MgH_2$, can store as much as 7.6 wt% $H_2$, but its thermodynamic stability is always the major problem in spite of the huge work focused on alloying and developing destabilization systems. Among these systems, Mg–Al–Li–Na–H has been reported to be very promising and many researchers focus their efforts on trying to understand reaction mechanisms and finding the best additives/catalysts to improve their hydrogen storage properties [3–11]. A comprehensive thermodynamic study is needed to find the best compositions in this system and to show their potential and limitations for hydrogen storage applications.

Recently Abdessameud et al. [12,13] used thermodynamic modeling to construct a database that describes the Mg–Al–Na–H system for hydrogen storage application. In this work, this database is extended to include Li in the system. This work is composed of two main parts; the first one consists of the assessment of the different binaries and ternaries in this system using CALPHAD method and FactSage software [14]. The second part focuses on the analysis of hydrogen storage properties of this system in comparison with the available experimental data and on the prediction of the most promising compositions in this system.

## 2. Literature review

### 2.1. Thermodynamic properties of Mg–Al–Li–Na–H system

The Mg–Al–Na–H system was reviewed and modeled in our previous papers [12,13]. In this section, a review of the remaining

* Corresponding author at: Department of Mechanical Engineering, Concordia University, 1455 de Maisonneuve Blvd West, Montreal, Quebec, Canada H3G 1M8.
*E-mail address:* mmedraj@encs.concordia.ca (M. Medraj).

http://dx.doi.org/10.1016/j.calphad.2016.06.001
0364-5916/

subsystems of the Mg–Al–Li–Na–H is presented.

No ternary compounds have been reported in the literature for the Al–Li–Na, Li–Mg–Na, and Li–Na–H systems. Since this work is oriented toward hydrogen storage properties, these ternaries are extrapolated from the constituent binaries using the CALPHAD method and are not included in this review.

### 2.1.1. Al–Li

A critical literature review and thermodynamic modeling of Al–Li system have been conducted by Saunders [15]. The phase diagram consists of liquid phase, terminal solid solutions fcc-Al and bcc-Li, a nonstoichiometric compound AlLi(η) and two stoichiometric compounds; $Al_2Li_3$ and $Al_4Li_9$. The liquid phase has been assessed using the substitutional solution model [15]. Harvey and Chartrand [16] used the Al–Li thermodynamic parameters published by Saunders [15] to predict the hydrogen solubility in liquid Al–Li alloys. They [16] found that the hydrogen solubility was overestimated and reassessed the Al–Li binary liquid using the modified quasichemical model and showed that Al–Li liquid alloys exhibit short range ordering. Their [16] model parameters for the liquid phase are used in this work.

Harvey [17] completed the assessment of the entire Al–Li system using the substitutional model for the terminal solid solutions fcc-Al and bcc-Li. Since the present work is dedicated to hydrogen storage applications, the fcc-Al and bcc-Li are remodeled in this work using the compound energy formalism (CEF), thus the model parameters published by Harvey [17] are changed accordingly. The thermodynamic model parameters for the compounds AlLi, $Al_2Li_3$ and $Al_4Li_9$ [17] are used in this work with minor changes in order to accommodate the newly modeled solid solutions; fcc-Al and bcc-Li. The calculated Al-Li phase diagram is presented in Fig. 1 and the parameters used are reported in Table 1.

### 2.1.2. Li–H

Harvey and Chartrand [16] assessed the Li-H system using the MQM for the liquid phase. The phase diagram consists of a gas phase, bcc-Li solid solution phase, a liquid phase with miscibility gap and a hydride phase, LiH. The model parameters used to describe the Li–H system by Harvey and Chartrand [16] are used in the present work except for the bcc-Li phase, which was remodeled using the CEF. The parameters used to describe the Li–H system are reported in Table 1 and the calculated Li–LiH phase diagram is presented in Fig. 2.

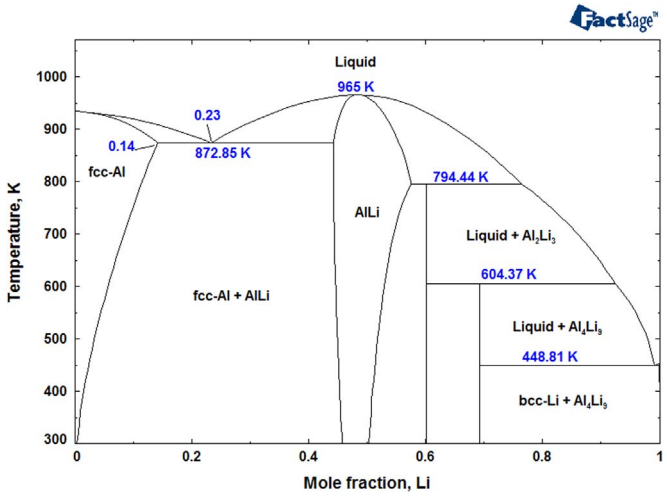


**Fig. 1.** The calculated Al–Li phase diagram at 1 bar.

### 2.1.3. Li–Mg

Nayeb-Hashemi et al. [18] reviewed the literature on the Li–Mg system and only the literature experimental data found by these authors [18] are used in the present optimization. The phase diagram consists of three phases: Liquid, hcp-Mg and bcc-Li terminal solid solutions. In the assessed phase diagram by Nayeb-Hashemi et al. [18], the maximum solid solubility of Li in Mg was 17 at% Li, the maximum solid solubility of Mg in Li was 75.5 at% Mg; and a eutectic reaction (L↔hcp-(Mg)+ bcc-(Li)) occurred at 23 at% Li and 861 K. The equilibrium diagram of the Li-Mg system has been widely investigated using different techniques [19–24].

Thermodynamic properties of the Li–Mg system have been investigated by Sommer [25], who measured the heat of mixing in the liquid phase at 940 K and by Saboungi and Blander [26], who measured Li activity in the Li–Mg liquid phase at 670, 735, 830 and 887 K. Gasior et al. [27] determined Li activities in solid and liquid Li–Mg alloys between 638 and 889 K.

Phase diagram calculations have been performed by Saboungi and Hsu [28], Nayeb-Hashemi et al. [18], Saunders [29], Gasior et al. [27], and most recently by Wang et al. [30]. In this work, the Li–Mg system is remodeled using the modified quasichemical model MQM for the liquid phase and CEF for the solid solutions for consistency with other systems in the same database. The results are discussed in more details in Section 4.1.1.

### 2.1.4. Li–Na

A critical review of the Li–Na system was reported by Bale [31]. This system exhibits extensive immiscibility in the liquid and the solid phases. A monotectic reaction takes place at 443.8 K and Na compositions 3.4 and 90.2 at% and a eutectic reaction at 365.3 K and 96.5 at% Na [31]. The consolute point has been calculated to be at 576.35 K (303.2 °C) and 35.7 at% Na. No thermodynamic data have been reported in the literature for the Li–Na system but the phase equilibria has been widely investigated using different techniques [31]. In the present study, the experimental data [32–39] selected by Bale [31] are used. Since no experimental evidence of solid solutions has been found in the literature, Li and Na mutual solubilities are considered negligible in the present work.

Pelton [40] and Zhang et al. [41] assessed the Li–Na system using substitutional solution model for the liquid and solid solution phases and using the critical review of Bale [31]. However, the system is re-modeled in this work using the MQM for the liquid phase and CEF for the solid solution for consistency with other binaries showing short range ordering. The modeling results of this system are discussed in Section 4.1.2.

### 2.1.5. Al–Li–Mg

Literature review of the Al–Li–Mg system was reported initially by Goel et al. [42] and Ghosh [43] and was then updated by Wang et al. [30]. Phase equilibria in this system were investigated by Schürmann and Voss [44] who designed a special apparatus to prepare Mg–Li–Al alloys. Phase analysis was performed by X-ray diffraction, optical metallography and electron probe microanalysis. However, Schürmann and Voss [44] did not include the $Al_4Li_9$ phase in their analysis of the Mg–Al–Li system and reported a ζ-phase ($Al_{11}Mg_{10}$), which is not considered as stable phase according to the widely accepted Al–Mg phase diagram [13].

Enthalpy of mixing of the Al–Li–Mg liquid was determined by Moser et al. [45] in the 869–1031 K temperature range using an isothermal high temperature mixing calorimeter. Schürmann and Geissler [46] constructed Al–Li–Mg isothermal sections at 473, 573, and 673 K (200, 300 and 400 °C) below 60 at% Li. Only one ternary stable compound τ ($Al_{53}Li_{33}Mg_{14}$) has been accepted in the literature [30,46]. Considerable solubility of Li in Al–Mg solid phases and of Mg in Al–Li solid phases has been reported in the literature [46,47]. In fact, Al–Mg compounds $Mg_{17}Al_{12}$(γ), $Mg_2Al_3$(β), and

**Table 1**
Optimized model parameters for the different phases in the Mg–Al–Li–Na–H system (G, Δg, and L in J/mole).

| | |
|---|---|
| ***Liquid phase (MQM)*** | [17] |
| $Z^{Al}_{AlLi} = Z^{Li}_{AlLi} = 2$, $\Delta g^{0}_{AlLi} = -25,597.8 + 15.012T - 0.1217TLnT$<br>$\Delta g^{10}_{AlLi} = -1.255T$; $\Delta g^{01}_{AlLi} = -14,126.8 + 10.3702T$ | |
| $Z^{Li}_{LiMg} = Z^{Mg}_{LiMg} = 6$, $\Delta g^{0}_{LiMg} = 3974.8 + 2.13T$; $\Delta g^{01}_{LiMg} = 0.698T$ | This work |
| $Z^{Li}_{LiNa} = Z^{Na}_{LiNa} = 6$, $\Delta g^{0}_{LiNa} = 3640.08$; $\Delta g^{10}_{LiNa} = 2698.68 - 3.033T$; $\Delta g^{01}_{LiNa} = 209.2$ | This work |
| $Z^{Li}_{LiH} = Z^{H}_{LiH} = 3$; $\Delta g^{0}_{LiH} = -106,697.2 + 33.85T - 1.58TLnT$<br>$\Delta g^{10}_{LiH} = 33,680.8 - 6.08T$; $\Delta g^{20}_{LiH} = -25,516.1$<br>$\Delta g^{30}_{LiH} = 7,040.9 + 5.97T$; $\Delta g^{01}_{LiH} = -55,745$ | [17] |
| ***Terminal solid solutions (Compound energy formalism)*** | This work |
| • hcp-(Mg) (Mg,Na,Al,Li)$_2$(H,Va)$_1$ | |
| ${}^{0}G^{Li_2H}_{Li:H} = 2G(Li_{hcp}) + 1/2G(H_2, gas)$; ${}^{0}G^{Li_2}_{Li:Va} = 2G(Li_{hcp})$<br>${}^{0}L^{hcp}_{Mg,Li:Va} = -13,879.36$; ${}^{1}L^{hcp}_{Mg,Li:Va} = 7,832.64$; ${}^{2}L^{hcp}_{Mg,Li:Va} = 7,832.64$<br>${}^{0}L^{hcp}_{Al,Li:Va} = -62,368$<br>${}^{0}L^{hcp}_{Na,Li:Va} = 40000$ | |
| • bcc-(Na) (Na,Mg,Al,Li)$_1$(H,Va)$_3$ | This work |
| ${}^{0}G^{LiH_3}_{Li:H} = G(Li_{bcc}) + 3/2G(H_2, gas) + 500,000$; ${}^{0}G^{Li}_{Li:Va} = G(Li_{bcc})$<br>${}^{0}L^{bcc}_{Mg,Li:Va} = -18,209.48 + 8.25T$; ${}^{1}L^{bcc}_{Mg,Li:Va} = 3481$;<br>${}^{2}L^{bcc}_{Mg,Li:Va} = 265$<br>${}^{0}L^{bcc}_{Li:H,Va} = 418,400$<br>${}^{0}L^{bcc}_{Na,Li:Va} = 20,920$ | |
| ${}^{0}L^{bcc}_{Al,Li:Va} = -27,000 + 8T$; $= {}^{2}L^{bcc}_{Al,Li:Va} 3,000$ | [15] |
| • fcc-Al (Al,Mg,Na,Li)$_1$(H,Va)$_1$ | This work |
| ${}^{0}G^{Li}_{Li:Va} = G(Li_{fcc})$; ${}^{0}G^{LiH}_{Li:H} = G(Al_{fcc}) + 1/2G(H_2, gas) + 500,000$<br>${}^{0}L^{fcc}_{Al,Li:Va} = -26,163.199 + 9.67T$ | |
| ***Nonstoichiometric compounds*** | [17] |
| $\gamma(Al12Mg17)$: $(Mg, Li)10(Al, Mg)24(Al, Mg)24$<br>$G^{\gamma}_{Li:Al:Mg} = 10G(Li_{bcc}) + 24G(Mg_{hcp}) + 24G(Al_{fcc}) - 64,310.4$<br>$G^{\gamma}_{Li:Mg:Al} = 10G(Li_{bcc}) + 24G(Mg_{hcp}) + 24G(Al_{fcc}) - 574,884.4 + 145.6032T$<br>$G^{\gamma}_{Li:Mg:Mg} = 10G(Li_{bcc}) + 48G(Mg_{hcp}) + 388,275.2$<br>$\beta(Al3Mg2)$: $(Al)19(Al, Mg, Li)2(Mg, Li)12$<br>$G^{\beta}_{Al:Mg:Li} = 2G(Mg_{hcp}) + 19G(Al_{fcc}) + 12G(Li_{bcc}) - 236,586.24 - 69.036T$<br>$G^{\beta}_{Al:Al:Li} = 21G(Al_{fcc}) + 12G(Li_{bcc}) - 236,586.24 - 69.036T$<br>$G^{\beta}_{Al:Li:Li} = 19G(Al_{fcc}) + 14G(Li_{bcc}) + 13,807.2$<br>$G^{\beta}_{Al:Li:Mg} = 12G(Mg_{hcp}) + 19G(Al_{fcc}) + 2G(Li_{bcc}) + 13,807.2$<br>$\eta$(AlLi): (Al, Li, Mg)1(Li, Mg, Va)1<br>$G^{AlLi}_{Al:Li} = -41,338 + 18.357T + G(Al_{fcc}) + G(Li_{bcc})$<br>$G^{AlLi}_{Al:Va} = 19,816 + G(Al_{fcc})$; $G^{AlLi}_{Li:Va} = 63,000^{*} + G(Li_{bcc})$; $G^{AlLi}_{Li:Li} = 2G(Li_{bcc})$<br>$G^{AlLi}_{Mg:Li} = -8,405 + 10.25T + G(Mg_{hcp}) + G(Li_{bcc})$<br>$G^{AlLi}_{Mg:Mg} = 8,368 + 2G(Mg_{hcp})$; $G^{AlLi}_{Mg:Va} = 4,184 + G(Mg_{hcp})$<br>$G^{AlLi}_{Al:Mg} = 8,293.3 - 8.368T + G(Al_{fcc}) + G(Mg_{hcp})$<br>$G^{AlLi}_{Li:Mg} = G(Li_{bcc}) + G(Mg_{hcp})$<br>${}^{0}L^{AlLi}_{Al,Li:Va} = 2,000$; ${}^{0}L^{AlLi}_{Al:Li,Va} = -24,418.4 + 9.58T^{*}$<br>${}^{0}L^{AlLi}_{Al,Li:Li} = 11,632$; ${}^{1}L^{AlLi}_{Al,Li:Li} = 20,000^{*}$ | |

**Table 1** (*continued*)

| | |
|---|---|
| ***Stoichiometric compounds:*** 298.15 K < $T$ < 1000 K (When not specified) | [17] |
| $G_{Al_2Li_3} = 2G(Al_{fcc}) + 3G(Li_{bcc}) - 89,690 + 33.96T$<br>$G_{Al_4Li_9} = 4G(Al_{fcc}) + 9G(Li_{bcc}) - 438,967.89 + 69.28T$ | |
| $G_{LiH} = -88,297.32 + 153.52T - 22.86T\ln T - 22.315 \times 10^{-3}T^2 - 5.89 \times 10^{-7}T^3 - 2,370\mathrm{Ln}T$<br>$G_{Al_{53}Li_{33}Mg_{14}} = 53G(Al_{fcc}) + 33G(Li_{bcc}) + 14G(Mg_{hcp}) - 1,324,573.135 + 2,729T$ | [17] |
| $G_{LiAlH4} = -330,533.6 + 4,817.71T - 811.34T\ln T + 1.23T^2 + 39.6 \times 10^{-5}T^3 + 8,948,260T^{-1}$ 298 K < $T$ < 500 K $G_{LiAlH4} = -132,001.66 + 206.9T - 38.11T\ln T - 0.081T^2 + 1.42 \times 10^{-5}T^3 - 461,924.05T^{-1}$ 500 K < $T$ < 800 K<br>$G_{Li3AlH6} = -331,337.95 + 674.27T - 110.34T\ln T - 0.081T^2 - 1.77 \times 10^{-6}T^3 + 446,400T^{-1} - 7,110\ln T$ | [59] |
| $G_{LiMg(AlH4)3} = G(LiH) + G(MgH2) + 3G(AlH3) + 37,221$<br>$G_{LiMgAlH6} = G(LiH) + G(MgH2) + G(AlH3) - 1,350$<br>$G_{Na2LiAlH6} = G(LiH) + G(NaH) + G(NaAlH4) - 36,124.41 + 47.91T$ | This work |

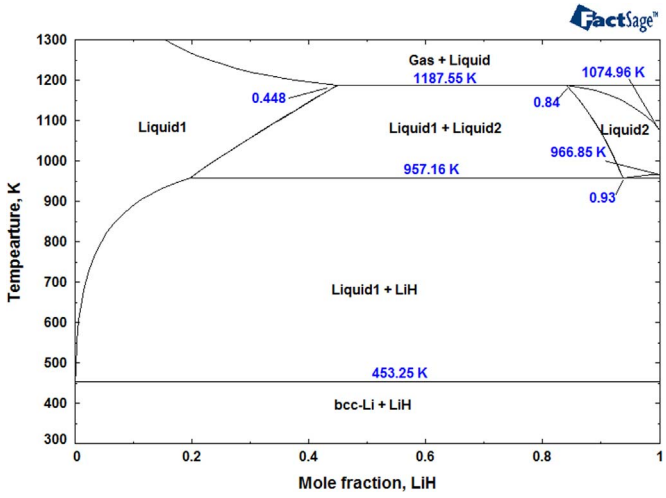


**Fig. 2.** The calculated Li–LiH phase diagram at 1 bar.

$Mg_{23}Al_{30}(\varepsilon)$ dissolve up to about 20 at% Li, 7 at% Li, and 0.8 at% Li, respectively [12,13]. LiAl(η) phase dissolves up to about 17 at% Mg [46,47].

Harvey [17] and Wang et al. [30] assessed the Al–Li–Mg system using the above-mentioned experimental data. Harvey [17] extrapolated the ternary liquid phase from the constituent binaries using mixed models (MQM for Al–Li and Al–Mg and substitutional solution model for Li–Mg) while Wang et al. [30] used substitutional solution model to extrapolate the liquid phase. In this work, the liquid phase is re-assessed using the MQM for all the binary liquids. No ternary interactions have been used in this work. The model parameters of Harvey [17] for the ternary compounds are used in this work with some modifications to attain consistency with the binary systems. The terminal solid solutions are re-modeled using the CEF.

### 2.1.6. Al–Li–H

Recently, Bodak and Perrot [48] conducted a literature review on the Al–Li–H system. Two ternary hydrides have been reported in the literature. $LiAlH_4$ ($P121/c1$ space group [49]) is not stable at room temperature but has a theoretical hydrogen capacity of 10.6 wt% $H_2$. $Li_3AlH_6$ ($R\bar{3}(148)$ space group [50]) is, in turn, stable and has a theoretical hydrogen capacity of 11.2 wt% $H_2$. $LiAlH_4$ decomposes in three steps [51] through reactions (1)–(3):

$$LiAlH_4 \rightarrow 1/3\ Li_3AlH_6 + 2/3Al + H_2\ 5.3\ \text{wt\%}\ H_2 \quad (1)$$

$$Li_3AlH_6 \rightarrow 3LiH + Al + 3/2H_2 + 2.6\ \text{wt\%}\ H_2 \quad (2)$$

$$3LiH + 3Al \rightarrow\ 3AlLi + 3/2\ H_2 + 2.6\ \text{wt\%}\ H_2 \quad (3)$$

Jang et al. [52] assessed the thermodynamic properties of the Al–Li–H hydrides using available experimental data [53–58]. These authors [52] presented two sets of thermodynamic parameters for $Li_3AlH_6$ because of the contradicting pressure composition isotherm (PCI) data of Chen et al. [57] and Brinks et al. [58]. Later, Grove et al. [59] reassessed the thermodynamic properties of $Li_3AlH_6$ hydride using thermal analysis data of Claudy et al. [54] and first principle predictions [50,60,61]. The results published by Grove et al. [59] showed very good agreement with the PCI results of Chen et al. [57]. The parameters adopted by Grove et al. [59] are used in this work. The ternary liquid is extrapolated from the constituent binaries.

### 2.1.7. Li–Mg–H

Experimentally verified ternary phases in the H–Li–Mg system could not be found in the literature. Li et al. [62] predicted by means of density functional theory (DFT) the thermodynamic stability of two lithium magnesium hydrides; $LiMgH_3$ and $Li_2MgH_4$; at 300 K. Recently, Meggiolaro et al. [63] predicted, using the same method, that these hydrides are metastable and spontaneously decompose to $MgH_2$ and LiH.

Ikeda et al. [64] studied the formation of perovskite-type structure in the $Li_xNa_{1-x}MgH_3$ ($x$=0, 0.17, 0.33, 0.50 and 1) hydride synthesized by ball milling NaH, $MgH_2$ and LiH. They did not observe the formation of $LiMgH_3$. For $x$=0, X-ray diffraction showed the diffraction peaks for the perovskite structure $NaMgH_3$, the position of these peaks shifted to higher angles indicating

partial substitution of Na by Li in the intermediate compositions ($x=0.17$, 0.33, and 0.50) but this shift disappeared after heat treatment of the samples [65]. These results [64,65] show that at equilibrium, Li cannot substitute Na in $NaMgH_3$ and thus, no stable ternary hydride exists in the Li–Mg–H system. Therefore, in this study, the model parameters describing the Li–Mg–H system have been extrapolated from the constituent binaries and no ternary hydride has been included.

#### 2.1.8. Quaternary phases

Three quaternary compounds, $LiMg(AlH_4)_3$, $LiMgAlH_6$, and $Na_2LiAlH_6$, have been reported in the literature for the Al–Li–Mg–Na–H system [6,59,66–69].

Lithium–magnesium alanate, $LiMg(AlH_4)_3$, ($P2_1/c(14)$ [69]) contains 9.7 wt% $H_2$ and has been found to decompose in two steps between 373 and 453 K (100 and 180 °C) [68]. Mamatha et al. [68] assumed that $LiMg(AlH_4)_3$ decomposes following Eqs. (4) and (5), where $LiMgAlH_6$ (space group $P321$ [69]) is an intermediate product of the decomposition of $LiMg(AlH_4)_3$. This assumption was based on the amount of hydrogen released in each step.

$$LiMg(AlH_4)_3 \rightarrow LiMgAlH_6 + 2Al + 3H_2 \ (4.8\ wt\%\ H_2) \quad (4)$$

$$LiMgAlH_6 \rightarrow LiH + MgH_2 + Al + 3/2H_2 \ (2.4\ wt\%\ H_2) \quad (5)$$

Mamatha et al. [68] showed, using DSC, that reaction (4) is exothermic, then not reversible, with an enthalpy value of −5 kJ/mol $H_2$ and reaction (5) is endothermic with an enthalpy of 8.7 kJ/mol $H_2$. Tang et al. [6] reported an enthalpy of −5.5 kJ/mol $H_2$ and of 13.1 kJ/mol $H_2$ for reactions (4) and (5), respectively. Tang et al. [6] reported that the results for reaction (5) agree with the results of Mamatha et al. [68]. Since Mamatha et al. [68] reported this enthalpy to be 8.7 kJ/mol $H_2$, this suggests that the value reported by Tang et al. [6] for reaction (5) (13.1 kJ/mol $H_2$) might be in (kJ/mol $LiMgAlH_6$). After dehydrogenation of $LiMg(AlH_4)_3$ to form $MgH_2$, LiH and Al (reactions (4) and (5)), Tang et al. [6] attempted the rehydrogenation of the products at 353 and 373 K (80 and 100 °C) under 190 bar of hydrogen for 24 h. These authors [6] found that neither $LiMgAlH_6$ nor $LiMg(AlH_4)_3$ form under these conditions.

Following the assessment of Grove et al. [59] for $LiMg(AlH_4)_3$ and $LiMgAlH_6$ hydrides, the above experimental data are adopted in this work to assess these two hydrides.

$Na_2LiAlH_6$ takes an ordered perovskite structure ($Fm\bar{3}m$ space group with a lattice constant of 7.4064(1) Å [67]) and decomposes reversibly to the binary hydrides following reaction (6) [66].

$$Na_2LiAlH_6 \rightarrow 2NaH + LiH + Al + 3/2H_2 \ (3.5\ wt\%\ H_2) \quad (6)$$

The enthalpy and/or entropy changes of reaction (6) were investigated using DSC [70,71] and PCI [66,67,72,73] measurements during dehydrogenation reactions. No assessment of the $Na_2LiAlH_6$ hydride has been reported in the literature. All these experimental data are used in the current work to establish a self-consistent database for the Mg–Al–Li–Na–H system.

### 2.2. Hydrogen storage properties

Recently, the hydrogen storage properties of the Mg–Al–Li–H system have been widely investigated [74–83]. Zhang et al. [74] and Chen et al. [76] investigated the hydrogen storage properties and reaction mechanisms of ball milled $MgH_2$–$LiAlH_4$ composites (with different molar ratios) using thermogravimetry (TG), differential scanning calorimetry (DSC), and XRD. Zhang et al. [74] also investigated the non-isothermal dehydrogenation of the composites: $MgH_2$–LiH, $MgH_2$–Al, and $MgH_2$–LiH–Al in comparison with $MgH_2$–$LiAlH_4$. The effect of additives on the hydrogen storage properties and reaction mechanisms of $MgH_2$–$LiAlH_4$ have been also investigated [77,78,81].

Liu et al. [75,79] investigated the $MgH_2$–$Li_3AlH_6$ composites using ball milling method, XRD analysis, thermogravimetry TGA, DSC, SEM and TEM. For comparison purposes, Liu et al. [75] investigated the dehydrogenation of $4MgH_2$–$LiAlH_4$ composite under the same conditions and showed that $Li_3AlH_6$ and $LiAlH_4$ have the same destabilization effect on $MgH_2$ (for 4:1 mol ratio of Mg to Al).

Recently, Yap et al. [82] and Juahir et al. [83] investigated the effect of dopants on the hydrogen storage properties and reaction mechanisms of $4MgH_2$–$Li_3AlH_6$ composites by the addition of 10 wt% of $K_2TiF_6$ and $Co_2NiO$. In all the reported results, the dehydrogenation temperatures in the mixtures, $MgH_2$–$LiAlH_4$ or $MgH_2$–$Li_3AlH_6$, were lower than those of the components and the kinetics was significantly improved. Two stages of dehydrogenation of $MgH_2$–$LiAlH_4$ or $MgH_2$–$Li_3AlH_6$ composites have been identified during the heating process:

For $MgH_2$–$LiAlH_4$ composites, the first stage has been attributed to the two-step decomposition of as-milled $LiAlH_4$ (reactions (1) and (2)) [74]. In $MgH_2$–$Li_3AlH_6$ composites the first stage has been attributed to the decomposition of $Li_3AlH_6$ (reaction (2)) [75]. The second stage has been attributed to the decomposition of $MgH_2$ and two different dehydrogenation routes have been reported:

$$4.08MgH_2 + 0.92LiH \rightarrow Li_{0.92}Mg_{4.08} + 4.54\ H_2 \quad (7)$$

$$17MgH_2 + 12\ Al \rightarrow Mg_{17}Al_{12} + 17H_2 \quad (8)$$

$$MgH_2 \rightarrow Mg + H_2 \quad (9)$$

The first route was proposed by Zhang et al. [74] who reported a mutual destabilization between $MgH_2$ and LiH to form $Li_{0.92}Mg_{4.08}$ intermediate phase in addition to the effect of Al on the dehydrogenation process of $MgH_2$ due to the formation of γ-phase ($Mg_{17}Al_{12}$). According to Zhang et al. [74] and many others [76,80–84], the second stage of dehydrogenation of $MgH_2$–$LiAlH_4$ or $MgH_2$–$Li_3AlH_6$ composites occurs following reactions (7) and (8). Mao et al. [77] identified the Li–Mg intermediate phase that resulted from the interaction of $MgH_2$ and LiH as $Li_3Mg_7$. In turn, Liu et al. [75,79] supported that LiH do not take part in the dehydrogenation reactions and the decomposition of $MgH_2$ proceeds following reactions (8) and (9). These authors argued that LiH could not be detected in XRD results because of its small amount and amorphous structure.

## 3. Thermodynamic modeling

The Mg–Al–Li–Na–H system is modeled in the current work using FactSage software [14]. The Gibbs energy functions of the pure elements (Al, Li, Mg, Na) are taken from the compilation of Dinsdale [85]. The Gibbs energy function of liquid monoatomic hydrogen estimated by Ransley and Talbot [86] is used in this work.

The liquid phase of the different binary systems is modeled using the modified quasichemical model MQM. Binary liquid parameters have been interpolated using the asymmetric Kohler–Toop technique where H is singled out as the asymmetric component [12,13]. No ternary parameters have been added to the liquid model.

Since hydrogen atoms occupy the interstitial positions in the terminal solid solutions fcc-Al, hcp-Mg, and bcc-Li/Na, these phases are modeled using the compound energy formalism. As discussed in

our previous papers [12,13] two sublattices: $(Al,Li,Mg,Na)_1(H,Va)_1$, $(Mg,Al,Li,Na)_2(H,Va)_1$, and $(Na,Li,Al,Mg)_1(H,Va)_3$ are used to describe these solid solutions, respectively, where Mg, Al, Li, and Na atoms mix randomly in the first sublattice to allow their mutual solubility and H atom and vacancy mix in the second sublattice.

The model parameters of the compounds: $Al_{30}Mg_{23}$, $AlH_3$, $MgH_2$, $Mg(AlH_4)_2$, NaH, $NaMgH_3$, $NaAlH_4$, $Na_3AlH_6$ have been cited in our previous papers [12,13] and those of the compounds: LiH [17], $Al_2Li_3$ [17], $Al_4Li_9$ [17], $Al_{53}Li_{33}Mg_{14}$ [17], $LiAlH_4$ [59], and $Li_3AlH_6$ [59] have been taken from the literature. $LiMg(AlH_4)_3$, $LiMgAlH_6$, and $Na_2LiAlH_6$ are modeled in this work as stoichiometric compounds based on literature data that are found reliable [6,59,66–69].

The nonstoichiometric compounds: β ($Al_3Mg_2$), γ ($Al_{12}Mg_{17}$), and AlLi are taken from Harvey [17] where they have been described by the sublattices: $(Mg,Li)_{10}(Al,Mg)_{24}(Al,Mg)_{24}$, $(Al)_{19}(Al,Mg,Li)_2(Mg,Li)_{12}$, and $(Al,Li,Mg)_1(Li,Mg,Va)_1$, respectively.

The gases: Al, $Al_2$, AlH, H, $H_2$, Li, $Li_2$, LiH, Mg, $Mg_2$, MgH, Na, $Na_2$, and NaH are included in this work and are considered ideal gases [12,13] because the non-ideal contribution of the pressure to the Gibbs energy, in the pressure range of interest, is very small. Gibbs energy functions of all the gases are taken from FactPS database [14].

When present in the assessed phase diagram, the gas phase refers to all the gases that form in the considered system and cited above. The pressure reported in all the figures is the total pressure of the system.

Thermodynamic equations used to model the different phases along with the model parameters of the Mg–Al–Na–H system have been reported in our previous papers [12,13]. The additional model parameters assessed in the current work are listed in Table 1.

## 4. Results and discussion

### 4.1. Thermodynamic properties of Mg–Al–Li–Na–H system

#### 4.1.1. Li-Mg

Fig. 3 shows the calculated Li–Mg phase diagram in comparison with experimental data. Good agreement can be seen between the calculated phase diagram and the selected experimental data except for the calculated solubilities of magnesium in bcc-Li which were lower than those measured by Freeth and Raynor [21]. This result was also found in the previous Li–Mg phase diagram calculations [18,27–30] and it was not possible, in this work, to find a set of parameters that reproduce the results of [21]. Freeth and Raynor [21] reported that quenching of a sample with bcc-Li phase at higher temperature causes the precipitation of the hcp-Mg phase and this might be the source of error in the determination of the boundary (hcp-Mg + bcc-Li)/(bcc-Li). General agreement exists between the calculated phase diagram in this work and in the assessment of Saunders [29]. In the Li-rich region of the liquidus in Fig. 3, the results by Henry and Cordiano [19] Grube et al. [20], and Feitsma et al. [22] have been chosen in this work for their close agreement and especially the resistivity measurements of Feitsma et al. [22] who determined the liquidus temperatures at 1 K intervals using high purity alloys.

The calculated Li solidus region of the phase diagram is in very good agreement with the results of Grube et al. [20]. As stated by Nayeb-Hashemi et al. [18] the lower solidus of Henry and Cordiano [19] has been caused by the segregation present in the alloys containing relatively high Li content.

The calculated heat of mixing for the liquid phase at 940 K is presented in comparison with the experimental data in Fig. 4. Better agreement exists between the calculated and the measured heat of mixing [25] than the results of Saunders [29], presented in dotted line in Fig. 4, with lower number of parameters. The calculated Li activities in the liquid phase at 670, 735, 830, and 887 K (not shown here) are very similar to the assessment of Saunders [29]. Both calculations show very good agreement with the experimental data [26].

#### 4.1.2. Li–Na

The calculated Li–Na phase diagram is presented in Fig. 5 where good agreement with the experimental data from the literature is shown. Since, no thermodynamic data have been found in the literature for this system, the model parameters have been selected to reproduce the liquid miscibility gap and the bcc (Li and Na) miscibility gap. The results obtained in this work are comparable to those obtained by Zhang et al. [41] and deviate slightly from those of Pelton [36]. In fact, the calculations of Zhang et al. [41] showed better agreement with the experimental data especially near the consolute point compared to the work of Pelton [40].

#### 4.1.3. Al–Li–Mg

The parameters used to model the Al–Li–Mg system are given in Table 1. As discussed in Section 2.1.5, Harvey [17] extrapolated the ternary liquid phase from the constituent binaries using the MQM for Al–Li and Al–Mg and substitutional solution model for Li–Mg. In this work, only the MQM is used; the model parameters of Harvey [17] for Al–Li and Al–Mg binary systems have been adopted and Li-Mg has been remodeled using the MQM in this work. As discussed in Section 2.1.5, the parameters used by Harvey [17] for the ternary compound τ ($Al_{53}Li_{33}Mg_{14}$) and the binary compounds (where solid solubility of the third element was considered) have been adopted in this work. The terminal solid solutions fcc-Al, hcp-Mg, and bcc-Li/Na have been remodeled using the CEF. The results (not shown here) are in reasonable agreement with experimental data and comparable to those obtained by Harvey [17] for the heat of mixing of liquid and Al–Li–Mg phase diagram. As discussed in Section 4.1.1, the calculated heat of mixing of Li–Mg liquid (using the MQM) show better agreement with the experimental data than the calculations done by Saunders [29] (which was used by Harvey [17] to extrapolate the ternary liquid in the assessment of Al–Li–Mg system). In this work, no improvement is shown with respect to the heat of mixing for the ternary liquid calculated by Harvey [17] because the available experimental data [41] covered only a small composition range.

The calculated isothermal sections at 473, 573, and 673 K (200, 300, and 400 °C) are in good agreement with the experimental data [46] and comparable with the results of Harvey [17]. The

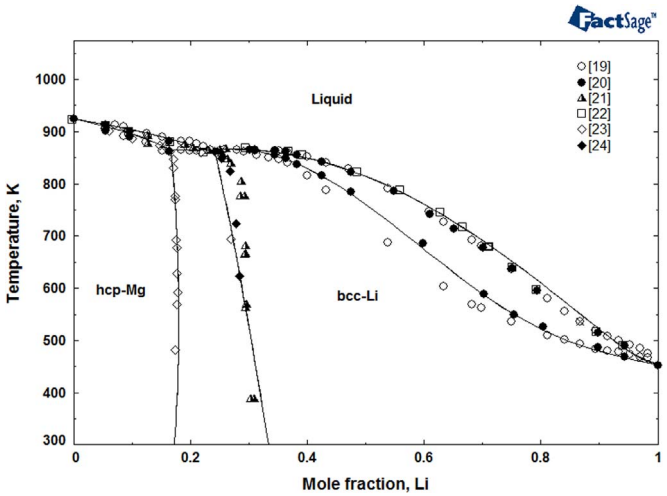


**Fig. 3.** Calculated Li–Mg phase diagram in comparison with experimental data from literature.

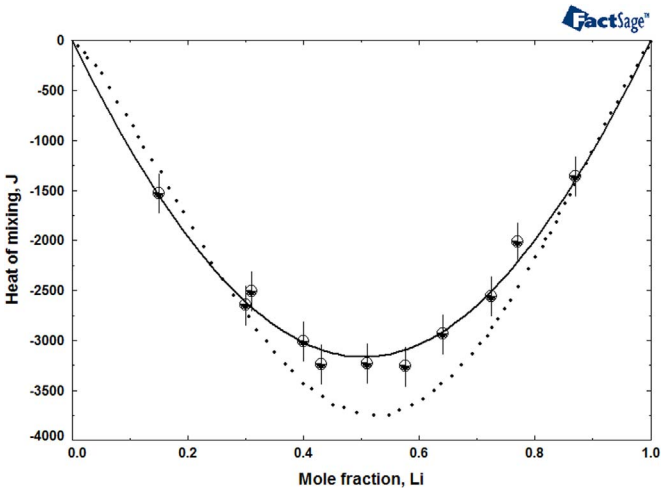


**Fig. 4.** Calculated heat of mixing for the liquid phase in the Li–Mg system at 940 K (full line) in comparison with experimental data [25] and the calculations made by saunders [29] (dotted line).

calculated isothermal section at 673 K (400 °C) is shown in Fig. 6.

#### 4.1.4. Al–Li–H

$LiAlH_4$ and $Li_3AlH_6$ hydrides are considered as stoichiometric compounds. The calculated pressure-temperature diagram and reaction path of $LiAlH_4$ composition are presented in Fig. 7. It should be noted that "Gas" phase in Fig. 7a refers to all the gases cited in Section 3 including $H_2$ whereas Fig. 7b shows the amount of released hydrogen. Fig. 7a shows that $LiAlH_4$ is not stable and do not form even at very high pressures. Jang et al. [52] reported that, according to their calculations, $Li_3AlH_6$ could absorb hydrogen to form $LiAlH_4$ at pressures above $10^3$ bar. However they [52] did not include $AlH_3$ hydride in their calculations. According to Fig. 7b, reaction (1) is spontaneous and $Li_3AlH_6$ decomposes reversibly according to reaction (2) to form LiH, fcc-Al, and $H_2$ at 69.9 °C and 1 bar. Some of the LiH decomposes at 573.6 °C accompanied with the formation of AlLi and $H_2$ according to Eq. (3). Based on the current work, the remaining LiH and AlLi both melt at around 674 °C forming two immiscible liquids. Liquid LiH (Liquid 2 in Fig. 7) decomposes gradually to form liquid phase at about 701 °C. Al and Li contents in fcc-Al, AlLi and Liquid phases are presented in Fig. 7b in dashed and dotted lines, respectively, in the same color as the corresponding phase. It shows that the gradual decrease in the amount of LiH is accompanied by an increase of the Li content in fcc-Al and of the released hydrogen when the temperature is increased. This proves that there is a destabilization effect between Al and LiH because of the solubility of Li in fcc-Al which reaches its maximum at 573.6 °C where AlLi forms. It can be seen in Fig. 7b that the amount of the formed AlLi and Li dissolved in it increase with temperature while the amount of Al dissolved in AlLi is constant and the amount of the remaining LiH decreases. This shows that AlLi destabilizes LiH because of the solubility of Li in AlLi.

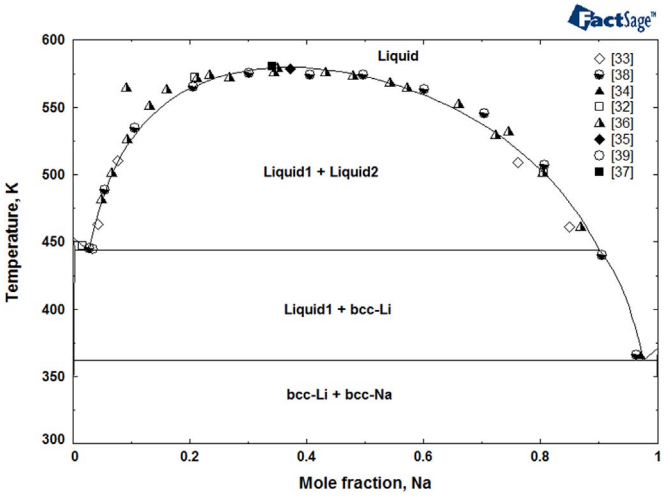


**Fig. 5.** The calculated Li–Na phase diagram at 1 bar compared with experimental data.

#### 4.1.5. Li–Mg–H

As discussed in Section 2.1.7, no experimentally confirmed ternary hydrides have been found in the Li–Mg–H system. However, some researchers reported a destabilization effect between Mg and LiH with the formation of Mg–Li compound $Li_{0.92}Mg_{4.08}$ as mentioned in Section 2.2.

The calculated Li–Mg phase diagram presented in Fig. 3 shows that the system is composed of only bcc-Li and hcp-Mg solid solutions, and that the solubility of Li in hcp-Mg is about 20 at% Li. The Mg–Li compound $Li_{0.92}Mg_{4.08}$ cited in the literature [74] has the same crystal structure as hcp-Mg solid solution and its composition approaches the solid solubility limit of Li in hcp-Mg, which suggests that, when mixed with Mg, Li from LiH hydride starts dissolving in Mg until its solubility limit of about 20 at%.

In order to investigate the effect of Mg on LiH, the calculated LiH-Mg phase diagram at 1 bar is shown in Fig. 8. Fig. 8 shows that LiH in the LiH–Mg mixture starts releasing hydrogen at 580.55 K (307.4 °C) and the produced Li is dissolved in hcp-Mg. As the temperature increases, the solubility limit of Li, stemming from LiH, in hcp-Mg increases (following the phase boundary hcp-Mg/hcp-Mg+LiH) until it reaches a maximum of 8.3 at% LiH at 891.65 K (618.5 °C). Fig. 8 shows that LiH hydride is too stable; only a very small amount decomposes because of the solubility of the produced Li in hcp-Mg.

#### 4.1.6. Quaternary hydrides

The quaternary compounds, $LiMg(AlH_4)_3$, $LiMgAlH_6$, and $Na_2LiAlH_6$ are considered in this work as stoichiometric compounds and their thermodynamic parameters are reported in Table 1. The assessment of $LiMg(AlH_4)_3$ and $LiMgAlH_6$ hydrides is performed based on the work of Grove et al. [59] and using the

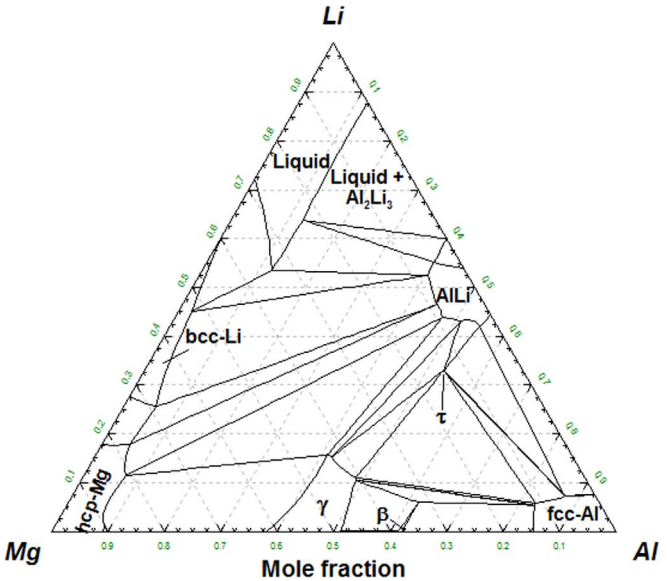


**Fig. 6.** The calculated Al–Li–Mg isothermal section at 673 K and 1 bar.

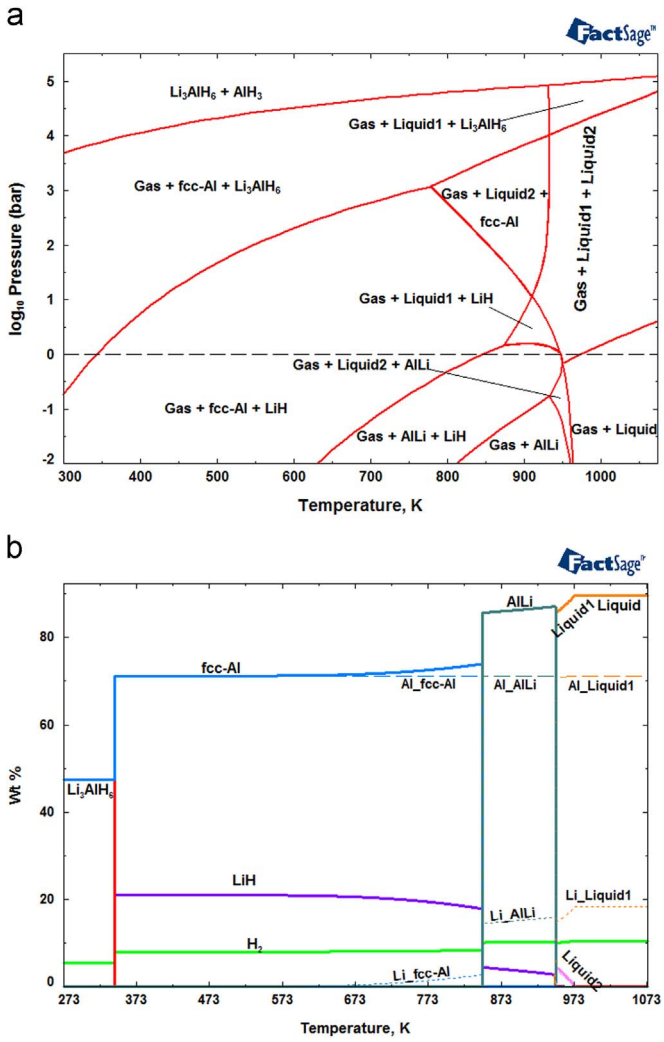


**Fig. 7.** Calculated (a) pressure–temperature diagram and (b) Reaction path at 1 bar, for $LiAlH_4$ composition.

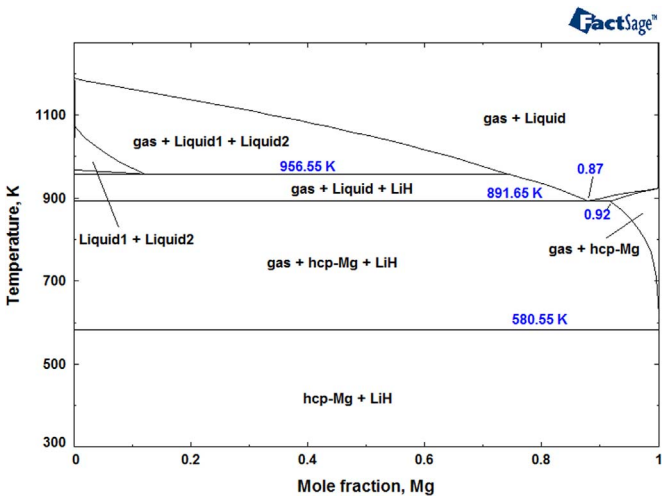


**Fig. 8.** The calculated Mg–LiH phase diagram at 1 bar.

experimental data reported by Mamatha et al. [68] and Tang et al. [6]. Fig. 9 presents the calculated pressure-temperature diagram for $LiMg(AlH_4)_3$ composition. Fig. 9 shows that the two compounds, $LiMg(AlH_4)_3$ and $LiMgAlH_6$, are not stable and then, reactions (4) and (5) are not reversible which is in very good agreement with the results of Tang et al. [6] Fig. 9 shows that, at 1 bar, $LiMg(AlH_4)_3$ decomposes spontaneously to form $Li_3AlH_6$, $MgH_2$, and fcc-Al.

$Na_2LiAlH_6$ is thermodynamically assessed for the first time in this work. Table 2 summarizes the calculated enthalpy and entropy of dehydrogenation of $Na_2LiAlH_6$, reaction (6), in comparison with experimental data from the literature.

It can be seen in Table 2 that Claudy et al. [70] and Huot et al. [71] reported different values for the enthalpy of reaction (6) using DSC experiments. It should be noted that the experimental conditions were also different. Huot et al. [71] realized his measurements under a hydrogen pressure of 2 bar and a heating rate of 10 K/min. Claudy et al. [70] experiments were under argon and with a heating rate of 1 K/min. The enthalpy and entropy values for reaction (6) obtained from pressure–composition isotherms (PCI) reported in Table 2 are also scattered. This can be explained by the poor kinetics of reaction (6), the long time needed to reach equilibrium and the slopped plateaus. Wang et al. [73] did not show PCI curves and reported a slightly higher enthalpy change than Claudy et al. [70]. Fossdal et al. [72], in turn, showed 5 PCI curves for catalyzed $Na_2LiAlH_6$ for temperatures between 443 and 523 K (170 and 250 °C). The plateaus were almost flat for high temperatures. Fossdal et al. [72] calculated two sets of values for enthalpy and entropy of reaction (6) reported in Table 2 using Van't Hoff plot. The results of Fossdal et al. [72] are in good agreement with Bogdanović et al. [66], who reported one PCI curve at 484 K (211 °C) showing an equilibrium pressure of about 13 bar. The PCIs reported by Graetz et al. [67] for catalyzed and uncatalyzed $Na_2LiAlH_6$ were slopped at low temperature with only two or three data points in the plateau region. Fig. 10 shows the calculated Van't Hoff plot for reaction (6) in comparison with PCI experimental data from the literature.

Good agreement can be seen between the calculated equilibrium pressures and the experimental data [67,72,87]. The calculated enthalpy of reaction (5) in the current work is lower but approaches more the enthalpy reported by Claudy et al. [70] using DSC measurements. The decomposition temperature of $Na_2LiAlH_6$ at 1 bar is calculated to be 417.23 K (144.1 °C).

### 4.2. Hydrogen storage properties

The calculated $MgH_2$–$LiAlH_4$ phase diagram at 1 bar is presented in Fig. 11a. It shows that $LiAlH_4$ decomposes spontaneously and the mixture is initially composed of fcc-Al solid solution, $MgH_2$, and $Li_3AlH_6$. At 343.03 K (69.9 °C), $Li_3AlH_6$ decomposes to

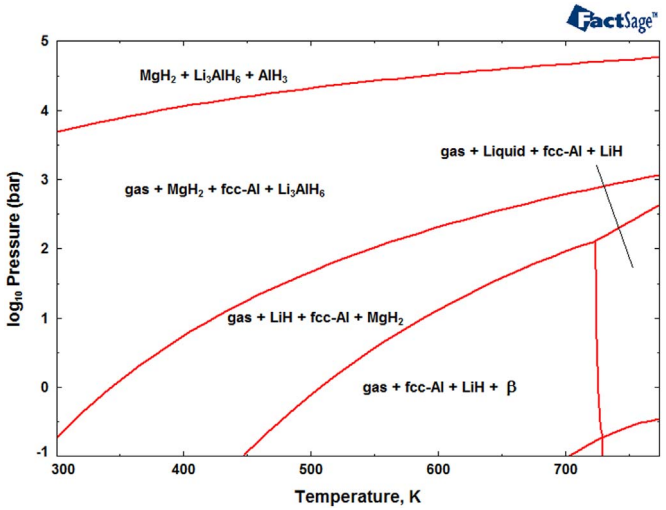


**Fig. 9.** Calculated pressure–temperature diagram of $LiMg(AlH_4)_3$.

**Table 2**
Enthalpy and entropy for reaction (6): $Na_2LiAlH_6 \rightarrow 2NaH + LiH + Al + 3/2H_2$.

| $\Delta H$ (kJ/mol $H_2$) | $\Delta S$ (J/K mol $H_2$) | Experiment | Reference |
|---|---|---|---|
| **60.75** | **145.1** | – | **This work** |
| 62.8 | – | DSC | [70] |
| 52.3 | – | PDSC (2 bar $H_2$) | [71] |
| 63.8 | 152.1 | PCI | [73] |
| $60.7 \pm 0.9$ | $146.5 \pm 1.9$ | PCI | [72] |
| $56.4 \pm 0.4$ | $137.9 \pm 0.7$ | PCI[a] | [72] |
| $53.5 \pm 1.2$ | $132.1 \pm 2.4$ | PCI | [67] |

[a] These values were found excluding the data point measured at 443 K.

form LiH and fcc-Al. The remaining phase transitions concern the decomposition of $MgH_2$–Al mixture, which depends on the atomic ratio of Mg and Al as discussed in our previous paper [13]. The phase diagram $MgH_2$–$Li_3AlH_6$ (not presented here) is similar to the phase diagram of $MgH_2$–$LiAlH_4$ with respect to phase relations which proves that dehydrogenation of Al–Li hydrides in the mixture is not affected by $MgH_2$ and that only the Al produced following their decomposition destabilizes $MgH_2$. Fig. 11a also shows that LiH does not take part in the dehydrogenation process of $MgH_2$. As discussed in Section 2.2, many authors have reported a destabilization effect between $MgH_2$ and LiH and claimed that this was due to the formation of Li-Mg compounds $Li_{0.92}Mg_{4.08}$ and $Li_3Mg_7$. However, $Li_{0.92}Mg_{4.08}$ and $Li_3Mg_7$ are not compounds in the widely accepted Li-Mg equilibrium phase diagram. In fact, Zhang et al. [74] identified, using XRD, two dehydrogenation stages in the $4MgH_2$–$LiAlH_4$ composites. The first stage was attributed to the two steps decomposition of $LiAlH_4$ (reactions (1) and (2)) and the second one to the decomposition of $MgH_2$ (reactions (6) and (7)) which means that the composite was composed of $Li_{0.92}Mg_{4.08}$ and γ phases. However, Zhang et al. [74] could detect LiH peaks in the XRD results of dehydrogenated state at 773 K (500 °C) for all the $MgH_2$–$LiAlH_4$ composites that they investigated. Ismail et al. [84] reported Mg as rehydrogenation product at 673 K (400 °C) besides $Li_{0.92}Mg_{4.08}$ and γ-phase for the same composite; $4MgH_2$–$LiAlH_4$, with the peaks of $Li_{0.92}Mg_{4.08}$ and Mg overlapping in the XRD patterns. Similar results have been reported by Chen et al. [76] for the $MgH_2$–$LiAlH_4$ composites with molar ratios 2.5:1 and 4:1 after dehydrogenation at 623 K (350 °C). For the composites with molar ratio 1:1, Chen et al. [76] reported that the peaks of $Li_{0.92}Mg_{4.08}$ or Mg could not be observed in the XRD results. In $TiF_3$–$MgH_2$–$LiAlH_4$ (0.05:1:1) composites, Mao et al. [77] identified γ as a dehydrogenation product at 673 K (400 °C),

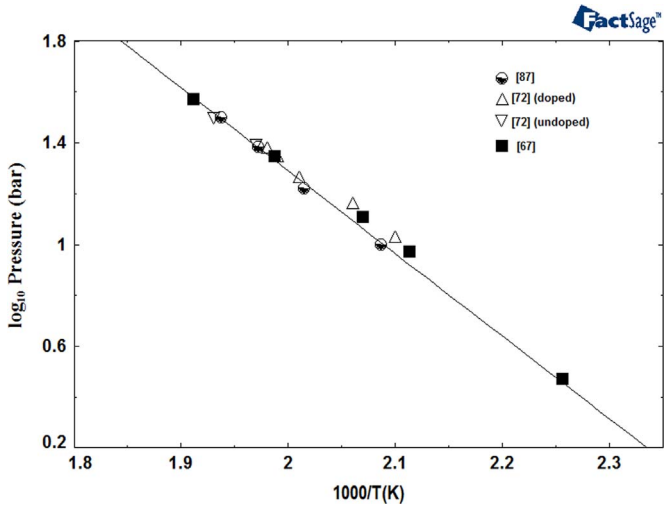


**Fig. 10.** The calculated Van't Hoff plot (solid line) for the dissociation of $Na_2LiAlH_6$ (reaction (6)).

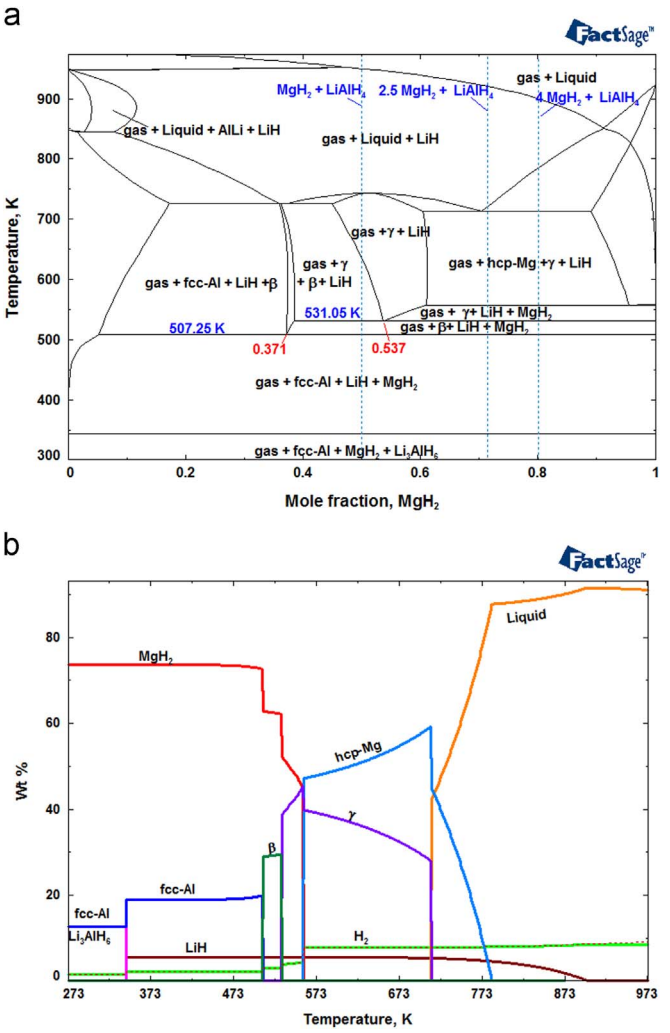


**Fig. 11.** (a) Calculated $MgH_2$–$LiAlH_4$ phase diagram at 1 bar, (b) Calculated reaction path of $4MgH_2$–$LiAlH_4$ composite at 1 bar.

and since no LiH was detected, they [77] identified $Mg_7Li_3$ as a possible product; they claimed that its peaks overlap with those of γ-phase in the XRD patterns.

The calculations shown in Fig. 11 are compared to the above-cited experimental data [74,76,77,84]. $MgH_2$–$LiAlH_4$ (4:1) and (2.5:1) composites correspond to 80 and 71.4 mol% $MgH_2$, respectively, in Fig. 11a, which shows that the dehydrogenation products of these composites at 673 K (400 °C) are γ, hcp-Mg, and LiH. For $MgH_2$–$LiAlH_4$ (1:1) composite, Fig. 11a shows that the dehydrogenation products are γ and LiH only.

The fact that the reported $Li_{0.92}Mg_{4.08}$ compound has the same crystal structure as hcp-Mg and its XRD peaks coincide with those of magnesium [76,84], suggests that the phase indexed as $Li_{0.92}Mg_{4.08}$ compound might be actually hcp-Mg solid solution and that, except the small solid solubility of Li (from LiH) in hcp-Mg (as discussed in Section 4.1.5), there is no destabilization effect between $MgH_2$ and LiH (reaction (6)). This suggestion is supported by the results of Chen et al. [76] who reported that, neither $Li_{0.92}Mg_{4.08}$ nor hcp-Mg were detected after dehydrogenation of $MgH_2$–$LiAlH_4$ (1:1) composite which is in very good agreement with the calculations shown in Fig. 11a. Also, the assumption of Mao et al. [77] concerning $Mg_7Li_3$ compound as a possible product (with XRD peaks overlapping with those of γ-phase) after dehydrogenation of $MgH_2$–$LiAlH_4$ (1:1) composite cannot be supported only by the fact that LiH peaks could not be detected in XRD results. In addition, Liu et al. [75,79] did not report any Mg-Li

phase in the dehydrogenation process of $MgH_2$–$LiAlH_4$/$Li_3AlH_6$ composites. These authors [75,79] argued that peaks of LiH are not detected in XRD results due to its small amount in comparison to Mg-related phases, its lower atomic number and amorphous structure. In fact, almost all the experimental data for $MgH_2$–$LiAlH_4$ composites reported that LiH is produced after rehydrogenation of the composites but its XRD peaks are hardly detected or overlapped by those of Al. Also, Zhang et al. [74] conducted isothermal dehydrogenation of $MgH_2$–LiH composite at 773 K (500 °C) and reported $Li_3Mg_7$ and $Li_{0.92}Mg_{4.08}$ as the decomposition products. However the hydrogen released from the sample did not exceeded 6 wt% $H_2$ [74] that is well below the hydrogen capacity of the composite (8.82 wt% $H_2$) and no other amorphous or unknown phases have been reported as other reaction products [74]. A reason for this inconsistency may be that only $MgH_2$ has decomposed (hcp-Mg could be indexed as $Li_{0.92}Mg_{4.08}$) and LiH could not be detected which explains the difference between the $H_2$ capacity of the composite and the amount of $H_2$ released and supports the results of this work. However, there is no other possible phase that could be indexed as $Li_3Mg_7$ in the decomposition products as reported by Zhang et al. [74].

The calculated reaction path of $4MgH_2$–$LiAlH_4$ composite is presented in Fig. 11b. In this figure, the released hydrogen $H_2$, which is part of the gas phase shown in Fig. 11a, is presented in green line and the gas phase is presented with a dotted line. Fig. 11b shows that $LiAlH_4$ decomposes spontaneously to form $Li_3AlH_6$ and fcc-Al and releases 1.4 wt% $H_2$. At 343.02 K (69.9 °C), $Li_3AlH_6$ decomposes to form LiH, fcc-Al and 0.7 wt% $H_2$.

It can be seen that during the two steps decomposition of $LiAlH_4$, $MgH_2$ does not play any role. From 343.03 K to 556.45 K (69.9 °C to 283.3 °C), $MgH_2$ is destabilized by the produced Al and decomposes in three steps: at 507.25 K (234.1 °C) to form β-phase, at 530.65 K (257.5 °C) to form γ-phase, and at 556.45 K (283.3 °C) to form hcp-Mg. Additional amounts of hydrogen of 0.07 wt% $H_2$, 1.56 wt% $H_2$, and 4 wt% $H_2$ are released in these steps, respectively. LiH does not contribute to these reactions. Fig. 11b shows a small gradual decrease in the amount of LiH between 556.45 K and 711.85 K (283.3 °C and 438.7 °C), which can be attributed to the destabilization effect of Mg as discussed in Section 4.1.5.

With increasing temperature from 556.45 K to 784.25 K (283.3 °C to 511.1 °C), 0.14 wt% $H_2$ is released gradually from the mixture. Finally at 899.55 K (626.4 °C), all the LiH has decomposed and a total amount of 8.57 wt% $H_2$ is released from the composite.

After rehydrogenation at 673 K (400 °C) and 4 MPa (40 bar), Zhang et al. [74] showed that the $4MgH_2$–$LiAlH_4$ composite contains $MgH_2$, LiH, and $Al_3Mg_2$ (β-phase). These authors [74] concluded that only $MgH_2$ is reversible in this composite with a loss in the hydrogen capacity because of the formation of β-phase. In turn, Chen et al. [76] reported that only $MgH_2$ and LiH can be reformed after rehydrogenation at 623 K (350 °C) and 10 MPa (100 bar) in the $4MgH_2$–$LiAlH_4$ composite. Liu et al. [75] showed that the mixture $4MgH_2$–$Li_3AlH_6$ is composed of $MgH_2$, Al, and LiH after rehydrogenation under 523 K (250 °C) and 2 MPa (20 bar) $H_2$. To analyze these different experimental results, the Pressure–Temperature (*P*–*T*) diagrams of the $4MgH_2$–$LiAlH_4$ composites are calculated in this work and presented in Fig. 12. The *P*–*T* diagrams of $4MgH_2$–$LiAlH_4$ and $4MgH_2$–$Li_3AlH_6$ are similar. Fig. 12 predicts the conditions (pressure and temperature) for the reversibility of the hydrogenation process of the composites $4MgH_2$–$LiAlH_4$/$Li_3AlH_6$. It can be seen that the calculations agree very well with all the cited experimental results [74–76] and give the conditions for the reversibility of the $4MgH_2$–$Li_3AlH_6$ composite. All the reported data for the undoped $MgH_2$–$LiAlH_4$ [74,76] and $MgH_2$–$Li_3AlH_6$ [75] show that the dehydrogenation kinetics and temperatures of these composites were improved in comparison with the composing hydrides and related these improvements to mutual catalytic effects between the hydrides. According to this work, $MgH_2$ does not affect the thermodynamics of $LiAlH_4$ and $Li_3AlH_6$ hydrides' decomposition and then, we can conclude that the improved reactions might be due to a catalytic effect of $MgH_2$. However, the improvement in $MgH_2$ decomposition is related to its destabilization by the resulting Al to form Mg–Al compounds, which with LiH might play a catalytic role on the decomposition of $MgH_2$.

The constructed database for the Mg–Al–Li–Na–H system allows predicting the dehydrogenation reaction mechanisms for all the possible composites in the system. According to our previous paper [13]. $MgH_2$ dehydrogenation occurs following reaction (10). It has been already proved [13] that destabilization of $MgH_2$ is due to the effect of Al. In the $MgH_2$–$LiAlH_4$/$Li_3AlH_6$ composites, Al is produced from the decomposition of $LiAlH_4$/$Li_3AlH_6$and $MgH_2$ decomposition route depends on the ratio of Mg to Al atoms [2]. Since $LiAlH_4$ is metastable, $Li_3AlH_6$ is preferable as Al source for its reversibility, its hydrogen content and low decomposition temperature. The dehydrogenation of $Li_3AlH_6$ proceeds according to reaction (11).

Fig. 11a shows that for Mg composition of 37.1 mol%, $MgH_2$ reacts with Al to form β-phase and releases all its hydrogen (6.07 wt% $H_2$) at 507.25 K (234.1 °C). For Mg composition of 53.7 mol%, $MgH_2$ reacts with β-phase to form γ-phase and releases all its hydrogen (6.36 wt% $H_2$) at 531.05 K (257.9 °C). It can be concluded that at these compositions, the maximum amount of hydrogen is released from the destabilized $MgH_2$. Reaction path of $MgH_2$–$Li_3AlH_6$ composites with $MgH_2$ content of 37.1 mol% and 53.7 mol% is calculated in this work at 1 bar and presented in Fig. 13.

$$MgH_2 \xrightarrow{557.8\ K} Mg + H_2\,(7.65\ wt\%\ H_2),\ \Delta H = 78.59\ KJ/mol\ H_2 \quad (10)$$

$$Li_3AlH_6 \xrightarrow{443.1\ K} 3LiH + Al + 1.5H_2 (5.6\ wt\%\ H_2),\ \Delta H = 33.90\ KJ/mol\ H_2 \quad (11)$$

We have already shown for the Mg–Al–Na–H system [13] that in $MgH_2$–$NaAlH_4$/$Na_3AlH_6$ composites, the component hydrides destabilize mutually and spontaneously to form a more stable hydride, $MgNaH_3$, which reduces significantly the hydrogen storage potential of the system.

As discussed in Section 4.1.6, there is only one stable quaternary hydride in the Mg–Al–Li–Na–H system, $Na_2LiAlH_6$, whose decomposition path and properties are given by reaction (12).

$$Na_2LiAlH_6 \xrightarrow{417.2\ K} Al + 2NaH + LiH + 1.5H_2 (3.52\ wt\%\ H_2),\ \Delta H = 61.83\ KJ/mol\ H_2 \quad (12)$$

Reaction (12) shows that this hydride might contribute to the destabilization of $MgH_2$ because of its decomposition products.

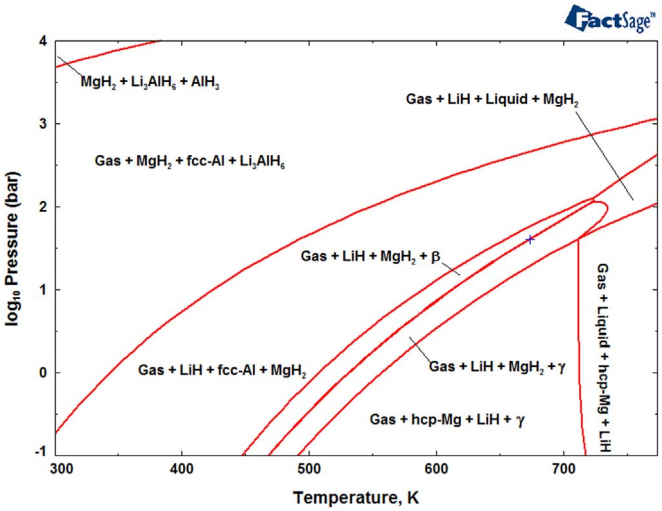


**Fig. 12.** Calculated pressure–temperature diagram of $4MgH_2$–$LiAlH_4$ composite.

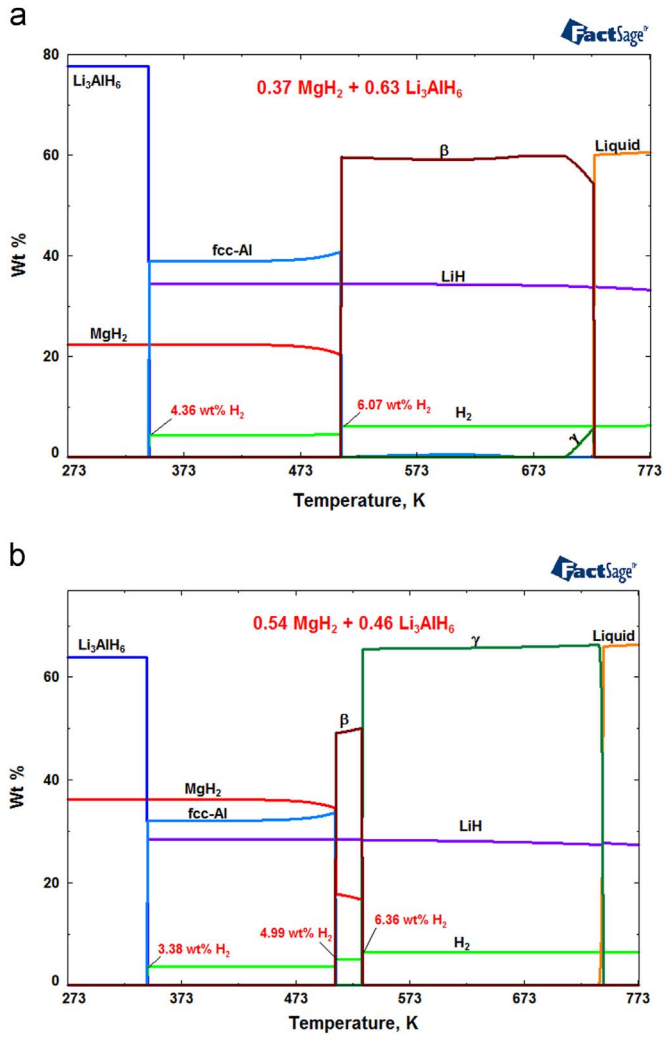


**Fig. 13.** Calculated reaction path of the most promising $MgH_2$–$Li_3AlH_6$ composites at 1 bar (a) $0.37MgH_2+0.63Li_3AlH_6$, (b) $0.54MgH_2+0.46Li_3AlH_6$.

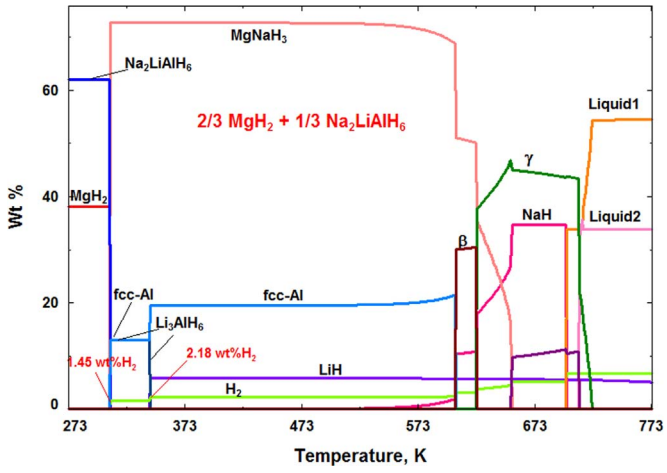


**Fig. 14.** Calculated reaction path of 2/3 $MgH_2+1/3$ $Na_2LiAlH_6$ composite at 1 bar.

According to the current thermodynamic modeling, $MgH_2$ and $Na_2LiAlH_6$, destabilize mutually at 308.4 K (35.25 °C) to form $MgNaH_3$. The maximum amount of hydrogen released at 308.4 K from $MgH_2/Na_2LiAlH_6$ composites is for $MgH_2$ content of 2/3 mol fraction. The reaction path of this composite at 1 bar is presented in Fig. 14. It shows that 1.45 wt% $H_2$ is released from the composite at 308.4 K (35.25 °C) where $MgNaH_3$, $Li_3AlH_6$, and fcc-Al form. A total of 2.19 wt% $H_2$ is released from the composite at 443.02 K (69.9 °C) following the decomposition of $Li_3AlH_6$. It can be concluded that even though $MgH_2$ and $Na_2LiAlH_6$ destabilize mutually and the decomposition temperature is reduced, the formation of $MgNaH_3$ reduces the hydrogen storage potential of the system.

As a result of this work and our previous results [12,13], it can be concluded that the addition of Na to Mg–Al–Li–H system leads to the formation of $MgNaH_3$ and thus reduces the potential of the system for mobile application according to the recommendation of DOE [88], and that more work is needed to improve the hydrogen storage properties of Mg–Al–Li–H system.

## 5. Conclusion

Thermodynamic modeling is used in this work to construct a database that describes the Mg–Al–Li–Na–H system in order to study its hydrogen storage properties. Since Mg–Al–Na–H system was studied before, only Li related binaries and ternaries are re-assessed in this paper. MQM and CEF are used to describe the liquid and the solid solution phases, respectively. Reaction pathways for $MgH_2$–$LiAlH_4/Li_3AlH_6$ composites are calculated and compared to the experimental data from the literature. A very good agreement has been found except for Li–Mg compounds reported in the literature. It is concluded that the reported $Li_{0.92}Mg_{4.08}$ is actually hcp-Mg, because the reported XRD peaks of this compound are identical to those of hcp-Mg and no compounds exist in the accepted Li–Mg phase diagram. Also, it is found that LiH is very stable and does not contribute to the decomposition reactions of $MgH_2$. Nevertheless, at high temperatures, a very small amount of Li from LiH dissolves in hcp-Mg and produces a negligible amount of $H_2$. In the composites $MgH_2$–$LiAlH_4/Li_3AlH_6$, Al produced from the decomposition of $LiAlH_4/Li_3AlH_6$ destabilized $MgH_2$ by the formation of β- and γ-phases. It is found that the re/dehydrogenation of the composites $MgH_2$–$Li_3AlH_6$ is reversible and that for $MgH_2$ content of 37.1 mol% and 53.7 mol%, 6.07 wt% $H_2$ (at 507.25 K (234.1 °C)) and 6.37 wt% $H_2$ (at 531.05 K (257.9 °C)) is released from the composite, respectively. A new destabilization reaction is predicted in this work between $MgH_2$ and $Na_2LiAlH_6$. These hydrides destabilize mutually at 308.4 K (35.25 °C) and 1 bar because of the formation of $MgNaH_3$. It is concluded that Na reduces considerably the hydrogen storage potential of the system.

## Acknowledgment

The authors acknowledge NSERC (Grant no. H2CAN350271) for financial support of the project through NSERC Hydrogen Canada Network ($H_2$Can).

## Appendix A. Supplementary material

Supplementary data associated with this article can be found in the online version at http://dx.doi.org/10.1016/j.calphad.2016.06.001.

## References

[1] R.J. Press, K.S.V. Santhanam, M.J. Miri, A.V. Bailey, G.A. Takacs, Introduction to Hydrogen Technology, 2009.
[2] P. Chen, M. Zhu, Recent progress in hydrogen storage, Mater. Today 11 (12) (2008) 36–43.

[3] Y.W. Cho, J. Shim, B. Lee, Thermal destabilization of binary and complex metal hydrides by chemical reaction: a thermodynamic analysis, Calphad 30 (1) (2006) 65–69.
[4] H. Liu, X. Wang, Y. Liu, Z. Dong, G. Cao, S. Li, M. Yan, Improved hydrogen storage properties of $MgH_2$ by ball milling with $AlH_3$: preparations, de/rehydriding properties, and reaction mechanisms, J. Mater. Chem. A 1 (2013) 12527–12535.
[5] M. Palumbo, F. Torres, J. Ares, C. Pisani, J. Fernandez, M. Baricco, Thermodynamic and ab initio investigation of the Al–H–Mg system, Calphad 31 (2007) 457–467.
[6] X. Tang, S.M. Opalka, B.L. Laube, F. Wu, J.R. Strickler, D.L. Anton, Hydrogen storage properties of Na–Li–Mg–Al–H complex hydrides, J. Alloy. Compd. 446 (2007) 228–231.
[7] J. Urgnani, M. Di Chio, M. Palumbo, M. Feuerbacher, J. Fernandez, F. Leardini, M. Baricco, Hydrogen absorption and desorption in rapidly solidified Mg-Al alloys, J. Phys. Conf. Ser. 144 (1) (2009) 12–16.
[8] D. Pottmaier, E.R. Pinatel, J.G. Vitillo, S. Garroni, M. Orlova, M.D. Baro, G.B. M. Vaughan, M. Fichtner, W. Lohstroh, M. Baricco, Structure and thermodynamic properties of the $NaMgH_3$ perovskite: a comprehensive study, Chem. Mater. 23 (2011) 2317–2326.
[9] M. Ismail, Y. Zhao, X. Yu, S. Dou, Improved hydrogen storage performance of $MgH_2$–$NaAlH_4$ composite by addition of $TiF_3$, Int. J. Hydrog. Energy 37 (2012) 8395–8401.
[10] M. Ismail, Y. Zhao, S. Dou, An investigation on the hydrogen storage properties and reaction mechanism of the destabilized $MgH_2$–$Na_3AlH_6$ (4:1) system, Int. J. Hydrog. Energy 38 (2013) 1478–1483.
[11] W. Hsu, C. Yang, C. Tan, W. Tsai, In situ synchrotron X-ray diffraction study on the dehydrogenation behavior of $LiAlH_4$–$MgH_2$ composites, J. Alloy. Compd. 599 (2014) 164–169.
[12] S. Abdessameud, M. Mezbahul-Islam, M. Medraj, Thermodynamic modeling of hydrogen storage capacity in Mg–Na alloys, Sci. World J. (2014), http://dx.doi.org/10.1155/2014/190320 (Article ID 190320, 16 pages).
[13] S. Abdessameud, M. Medraj, Understanding the hydrogen storage behavior of promising Al–Mg–Na compositions using thermodynamic modeling, Mater. Renew. Sustain. Energy 5 (2) (2016) 1–29.
[14] C. Bale, A. Pelton, W. Thompson, FactSage 6.4, FactSage thermochemical software and databases, 2013. ⟨http://www.crct.polymtl.ca/⟩.
[15] N. Saunders, Calculated stable and metastable phase equilibria in Al–Li–Zr alloys, Z. Metall. 80 (1989) 894–903.
[16] J.P. Harvey, P. Chartrand, Modeling the hydrogen solubility in liquid aluminum alloys, Metall. Mater. Trans. 41B (2010) 908–924.
[17] J. Harvey, Developpement d'une base de donnees thermodynamique pour la modelisation de la solubilite d'hydrogene dans les alliages d'aluminium, ProQuest Dissertations and Theses, Ecole Polytechnique, Montreal, Canada, M.Sc. A., 2007.
[18] A. Nayeb-Hashemi, J. Clark, A. Pelton, The Li–Mg (lithium-magnesium) system, J. Ph. Equilib. 5 (1984) 365–374.
[19] O.H. Henry, H.V. Cordiano, The lithium-magnesium equilibrium diagram, Trans. AIME 101 (1934) 319–332.
[20] G. Grube, H. Zeppelin, H. Bumm, Elektrische leitfähigkeit und zustandsdiagramm bei binären legierungen. 11. Mitteilung. das system lithium-magnesium, Z. Elektrochem. Angew. Phys. Chem. 40 (1934) 160–164.
[21] W. Freeth, G. Raynor, The systems magnesium-lithium and magnesium-lithium-silver, J. Inst. Met. 82 (1954) 575–580.
[22] P. Feitsma, T. Lee, W. Van der Lugt, Electrical transport properties and phase diagram of the liquid binary lithium-magnesium system, Physica B C 93 (1978) 52–58.
[23] W. Hume-Rothery, G. Raynor, E. Butchers, Equilibrium relations and some properties of magnesium-lithium and magnesium-silver-lithium alloys, J. Inst. Met. 71 (1945) 589–601.
[24] J. Catterall, Solubility of magnesium in lithium, Nature 169 (1952) 336.
[25] F. Sommer, Thermodynamic investigation of liquid Li–Mg alloys, Z. Metall. 70 (1979) 359–361.
[26] M. Saboungi, M. Blander, Electromotive force measurements in molten lithium-magnesium alloys, J. Electrochem. Soc. 122 (1975).
[27] W. Gasior, Z. Moser, W. Zakulski, G. Schwitzgebel, Thermodynamic studies and the phase diagram of the Li–Mg system, Metall. Mater. Trans. A 27 (1996) 2419–2428.
[28] M. Saboungi, C.C. Hsu, Computation of isothermal sections of the Al–Li–Mg system, Calphad 1 (1977) 237–251.
[29] N. Saunders, A review and thermodynamic assessment of the Al–Mg and Mg–Li systems, Calphad 14 (1990) 61–70.
[30] P. Wang, Y. Du, S. Liu, Thermodynamic optimization of the Li–Mg and Al–Li–Mg systems, Calphad 35 (2011) 523–532.
[31] C. Bale, The Li–Na (lithium–sodium) system, J. Ph. Equilib. 10 (1989) 265–268.
[32] H. Schürmann, R. Parks, Paraconductivity in binary metallic liquids above the critical point, Phys. Rev. Lett. 27 (26) (1971) 1790–1793.
[33] P. Feitsma, J. Hallers, F. Werff, W. Van der Lugt, Electrical resistivities and phase separation of liquid lithium-sodium alloys, Physica B C 79 (1975) 35–52.
[34] M.G. Down, P. Hubberstey, R.J. Pulham, Sodium–lithium phase diagram: redetermination of the liquid immiscibility system by resistance measurement, J. Chem. Soc., Dalton Trans. 14 (1975) 1490–1492.
[35] H. Endo, H. Hoshino, K. Tamura, M. Mushiage, Phase separation of liquid binary mixtures containing metals under pressure, Solid State Commun. 32 (1979) 1243–1246.
[36] F.A. Kanda, R.C. Faxon, D.V. Keller, The determination of the liquid immiscibility boundaries of the lithium–sodium and thallium–selenium systems by the liquid density method, Phys. Chem. Liq. 1 (1968) 61–72.
[37] E. Wu, H. Brumberger, Critical small-angle X-ray scattering of the liquid sodium–lithium system, Phys. Lett. A 53 (1975) 475–477.
[38] O. Salmon, D. Ahmann, The lithiuim–sodium liquid metal system, J. Phys. Chem. 60 (1956) 13–14.
[39] W. Howland, L. Epstein, The binary system sodium–lithium, Adv. Chem. Ser. 19 (1957) 34–41.
[40] A.D. Pelton, Calculation of phase equilibria and thermodynamic properties of the Li-Na-H system, Z. Metall./Mater. Res. Adv. Tech. 84 (1993) 767–772.
[41] S. Zhang, D. Shin, Z. Liu, Thermodynamic modeling of the Ca–Li–Na system, Calphad 27 (2003) 235–241.
[42] N. Goel, J. Cahoon, The Al-Li-Mg system (aluminum–lithium–magnesium), Bull. Alloy. Ph. Diagr. 11 (1990) 528–546.
[43] G. Ghosh, Aluminium-lithium-magnesium. in: MSIT Ternary Evaluation Program, in MSIT Workplace, 48, MSI, Materials Science International Services GmbH, Stuttgart, 1993, Document ID: 10.12175.1.20, (Crys. Structure, Equi. Diagr., Assess).
[44] E. Schürmann, H. Voss, Investigation of the melting equilibria of Mg–Li–Al alloys, Giessereiforschung 33 (1981) 33–53.
[45] Z. Moser, R. Agarwal, F. Sommer, B. Predel, Calorimetric studies of liquid Al–Li–Mg alloys, Z. Metall. 82 (1991) 317–321.
[46] E. Schürmann, I. Geissler, Solid phase equilibrium in Mg-Rich alloys of the Al–Li–Mg system, Giessereiforschung 32 (1980) 163–174.
[47] H. Voss, Development of an Apparatus for Melting Lithium-Containing Magnesium-Aluminium Alloys and their Use in Thermal Analysis (thesis), Tech. Univ.Clausthal, Clausthal, Germany 1979, p. 82.
[48] O. Bodak, P. Perrot, Al–H–Li, in: G. Effenberg, S. Ilyenko (Eds.), Light Metal Ternary Systems: Phase Diagrams, Crystallographic and Thermodynamic Data, Landolt-Börnstein - Group IV Physical Chemistry,, 11A3, Springer-Verlag Berlin Heidelberg, Germany, 2005, pp. 58–63.
[49] N. Sklar, B. Post, Crystal structure of lithium aluminum hydride, Inorg. Chem. 6 (4) (1967) 669–671.
[50] S. Chung, H. Morioka, Thermochemistry and crystal structures of lithium, sodium and potassium alanates as determined by ab initio simulations, J. Alloy. Compd. 372 (2004) 92–96.
[51] W. Garner, E. Haycock, The thermal decomposition of lithium aluminium hydride, Pro. Roy. Soc. Lond. A: Math. Phys. Eng. Sci. 211 (1106) (1952) 335–351.
[52] J. Jang, J. Shim, Y.W. Cho, B. Lee, Thermodynamic calculation of $LiH \leftrightarrow Li_3AlH_6 \leftrightarrow LiAlH_4$ reactions, J. Alloy. Compd. 420 (2006) 286–290.
[53] M.B. Smith, G.E. Bass Jr, Heats and free energies of formation of the alkali aluminum hydrides and of cesium hydride, J. Chem. Eng. Data 8 (1963) 342–346.
[54] P. Claudy, B. Bonnetot, J. Letoffe, G. Turck, Determination of thermodynamic constants of simple and complex hydrides of aluminum, 4. Enthalpy of formation of $LiAlH_4$ and $Li_3AlH_6$, Thermochim. Acta 27 (1–3) (1978) 213–221.
[55] A.J. Bard, R. Parsons, J. Jordan, Standard Potentials in Aqueous Solution, 1985.
[56] T.N. Dymova, D.P. Aleksandrov, V.N. Konoplev, Spontaneous and thermal decomposition of lithium tetrahydroaluminate $LiAlH_4$: the promoting effect of mechanochemical action on the process, Russ. J. Coord. Chem. 20 (4) (1994) 279–285.
[57] J. Chen, N. Kuriyama, Q. Xu, H.T. Takeshita, T. Sakai, Reversible hydrogen storage via titanium-catalyzed $LiAlH_4$ and $Li_3AlH_6$, J. Phys. Chem. B 105 (45) (2001) 11214–11220.
[58] H. Brinks, A. Fossdal, J. Fonneløp, B. Hauback, Crystal structure and stability of $LiAlD_4$ with $TiF_3$ additive, J. Alloy. Compd. 397 (2005) 291–295.
[59] H. Grove, O.M. Løvvik, W. Huang, S.M. Opalka, R.H. Heyn, B.C. Hauback, Decomposition of lithium magnesium aluminum hydride, Int. J. Hydrog. Energy 36 (2011) 7602–7611.
[60] O. Løvvik, S.M. Opalka, H.W. Brinks, B.C. Hauback, Crystal structure and thermodynamic stability of the lithium alanates $LiAlH_4$ and $Li_3AlH_6$, Phys. Rev. B 69 (13) (2004) 134117(1-9).
[61] J.K. Kang, J.Y. Lee, R.P. Muller, W.A. Goddard III, Hydrogen storage in LiAlH4: predictions of the crystal structures and reaction mechanisms of intermediate phases from quantum mechanics, J. Chem. Phys. 121 (2004) 10623–10633.
[62] D. Li, T. Zhang, S. Yang, Z. Tao, J. Chen, Ab initio investigation of structures, electronic and thermodynamic properties for Li–Mg–H ternary system, J. Alloy. Compd. 509 (2011) 8228–8234.
[63] D. Meggiolaro, G. Gigli, A. Paolone, F. Vitucci, S. Brutti, Incorporation of lithium by $MgH_2$: an ab initio study, J. Phys. Chem. C 117 (2013) 22467–22477.
[64] K. Ikeda, Y. Kogure, Y. Nakamori, S. Orimo, Formation region and hydrogen storage abilities of perovskite-type hydrides, Prog. Solid State Chem. 35 (2007) 329–337.
[65] K. Ikeda, Y. Nakamori, S. Orimo, Formation ability of the perovskite-type structure in $Li_xNa_{1-x}MgH_3$ ($x$=0, 0.5 and 1.0), Acta Mater. 53 (2005) 3453–3457.
[66] B. Bogdanović, M. Schwickardi, Ti-doped alkali metal aluminium hydrides as potential novel reversible hydrogen storage materials, J. Alloy. Compd. 253 (1997) 1–9.
[67] J. Graetz, Y. Lee, J. Reilly, S. Park, T. Vogt, Structures and thermodynamics of the mixed alkali alanates, Phys. Rev. B 71 (18) (2005) 184115(1-7).
[68] M. Mamatha, B. Bogdanović, M. Felderhoff, A. Pommerin, W. Schmidt, F. Schüth, C. Weidenthaler, Mechanochemical preparation and investigation of properties of magnesium, calcium and lithium–magnesium alanates, J. Alloy. Compd. 407 (1) (2006) 78–86.

[69] H. Grove, H. Brinks, R. Heyn, F. Wu, S. Opalka, X. Tang, B. Laube, B. Hauback, The structure of $LiMg(AlD_4)_3$, J. Alloy. Compd. 455 (1) (2008) 249–254.
[70] P. Claudy, B. Bonnetot, J. Bastide, L. Jean-Marie, Reactions of lithium and sodium aluminium hydride with sodium or lithium hydride. Preparation of a new alumino-hydride of lithium and sodium $LiNa_2AlH_6$, Mater. Res. Bull. 17 (1982) 1499–1504.
[71] J. Huot, S. Boily, V. Güther, R. Schulz, Synthesis of $Na_3AlH_6$ and $Na_2LiAlH_6$ by mechanical alloying, J. Alloy. Compd. 283 (1) (1999) 304–306.
[72] A. Fossdal, H. Brinks, J. Fonneløp, B. Hauback, Pressure–composition isotherms and thermodynamic properties of $TiF_3$-enhanced $Na_2LiAlH_6$, J. Alloy. Compd. 397 (1) (2005) 135–139.
[73] P. Wang, L. Ma, Z. Fang, X. Kang, P. Wang, Improved hydrogen storage property of Li–Mg–B–H system by milling with titanium trifluoride, Energy Environ. Sci. 2 (2009) 120–123.
[74] Y. Zhang, Q.F. Tian, S.S. Liu, L.X. Sun, The destabilization mechanism and de/re-hydrogenation kinetics of $MgH_2$–$LiAlH_4$ hydrogen storage system, J. Power Sour. 185 (2008) 1514–1518.
[75] S. Liu, L. Sun, J. Zhang, Y. Zhang, F. Xu, Y. Xing, F. Li, J. Zhao, Y. Du, W. Hu, Hydrogen storage properties of destabilized $MgH_2$–$Li_3$ $AlH_6$ system, Int. J. Hydrog. Energy 35 (15) (2010) 8122–8129.
[76] R. Chen, X. Wang, L. Xu, L. Chen, S. Li, C. Chen, An investigation on the reaction mechanism of $LiAlH_4$–$MgH_2$ hydrogen storage system, Mater. Chem. Phys. 124 (1) (2010) 83–87.
[77] J. Mao, Z. Guo, X. Yu, M. Ismail, H. Liu, Enhanced hydrogen storage performance of $LiAlH_4$–$MgH_2$–$TiF_3$ composite, Int. J. Hydrog. Energy 36 (9) (2011) 5369–5374.
[78] M. Ismail, Y. Zhao, X. Yu, J. Mao, S. Dou, The hydrogen storage properties and reaction mechanism of the $MgH_2$–$NaAlH_4$ composite system, Int. J. Hydrog. Energy 36 (2011) 9045–9050.
[79] S. Liu, L. Sun, F. Xu, J. Zhang, Z. Cao, Y. Liu, Improved dehydrogenation of $MgH_2$–$Li_3AlH_6$ mixture with $TiF_3$ addition, Int. J. Hydrog. Energy 36 (18) (2011) 11785–11793.
[80] Q. Wan, P. Li, Z. Li, F. Zhai, X. Qu, A.A. Volinsky, Improved hydrogen storage performance of $MgH_2$–$LiAlH_4$ composite by addition of $MnFe_2O_4$, J. Phys. Chem. C 117 (51) (2013) 26940–26947.
[81] N.S. Mustafa, M. Ismail, Enhanced hydrogen storage properties of $4MgH_2$ $+LiAlH_4$ composite system by doping with $Fe_2O_3$ nanopowder, Int. J. Hydrog. Energy 39 (15) (2014) 7834–7841.
[82] F.H. Yap, M. Ishak, M. Ismail, Enhanced hydrogen storage performance of destabilized $4MgH_2$–$Li_3AlH_6$ system doped with $Co_2NiO$ nanopowder, Int. J. Hydrog. Energy 40 (32) (2015) 10131–10138.
[83] N. Juahir, F.H. Yap, N. Mustafa, M. Ismail, Hydrogen storage properties of $4MgH_2$–$Li_3AlH_6$ composite improved by the addition of $K_2TiF_6$, Int. J. Hydrog. Energy 40 (37) (2015) 12713–12720.
[84] M. Ismail, Y. Zhao, X. Yu, S. Dou, Effect of different additives on the hydrogen storage properties of the $MgH_2$-$LiAlH_4$ destabilized system, RSC Adv. 1 (3) (2011) 408–414.
[85] A.T. Dinsdale, SGTE data for pure elements, Calphad 15 (1991) 317–425.
[86] C. Ransley, D. Talbot, Hydrogen porosity in metals with special reference to aluminum and its alloys, Z. Metall. 46 (5) (1955) 328–337.
[87] F. Wang, Y. Liu, M. Gao, K. Luo, H. Pan, Q. Wang, Formation reactions and the thermodynamics and kinetics of dehydrogenation reaction of mixed alanate Na2LiAlH6, J. Phys. Chem. C 113 (2009) 7978–7984.
[88] L. Klebanoff, J. Keller, 5 years of hydrogen storage research in the US DOE metal hydride center of excellence (MHCoE), Int. J. Hydrog. Energy 38 (11) (2013) 4533–4576.